Available online at www.sciencedirect.com
ScienceDirect
International Journal of Heat and Mass Transfer 51 (2008) 2834–2846
International Journal of HEAT and MASS TRANSFER
www.elsevier.com/locate/ijhmt

Performance of two equation turbulence models for prediction of flow and heat transfer over a wall mounted cube

G. Seeta Ratnam, S. Vengadesan *

Department of Applied Mechanics, IIT Madras, Chennai, India

Received 16 March 2007; received in revised form 17 August 2007
Available online 19 November 2007

Abstract

This paper deals with the CFD predictions of the three dimensional incompressible flow over a wall mounted cubic obstacle placed in fully developed turbulent flow along with the heat transfer calculations. Reynolds number considered in this study is 1870 based on cube height, h and bulk velocity U_b. Our main objective is to find out the appropriate two equation turbulence model for the complex flow structure which involves recirculation, separation and reattachment. We have used standard k–ε, low-Reynolds number k–ε, non-linear k–ε model, standard k–ω and improved k–ω models to solve the closure problem. The non-linear k–ε model and improved k–ω models along with standard models are validated with bench mark problem – flow through a backward facing step (BFS). Results showed that the improved k–ω model is giving overall better predictions of the flow field especially recirculation zone, mean streamwise velocity, and turbulent characteristics when compared to those by standard eddy viscosity models. The non-linear k–ε model is giving better prediction when compared to standard k–ε and low Reynolds number k–ε models. The complex vortex structure around the cube causes large variation in the local convective heat transfer coefficient. The maximum of the heat transfer coefficient occurred in the proximity of the reattachment points and the minimum is found at the recirculation zone.

Keywords: Three dimensional bluff body; Horseshoe vortex; Arch vortex; Two equation turbulence models; Local convective heat transfer coefficient

1. Introduction

The study of the flow around surface mounted, sharp edged obstacles placed in a channel is fundamental to the understanding of the flow mechanics for complex two- and three-dimensional geometries. This flow field has features like flow separation, reattachment and recirculation. Investigation on the heat transfer from the surfaces of a wall mounted bluff bodies in turbulent flow is still a challenging and has significant importance in many technological applications.

Notable examples are electronic components attached to a printed circuit board in electronic equipment and gas turbine blade cooling. The temperature control of critical components is essential for optimum board and system performance since local overheating is still a major cause of the failure. Similar problems can be found in gas turbines. Turbine blades are frequently cooled by cold fluid circulating through internal passages equipped with wall mounted protruding ribs. Inefficient cooling can lead to local blade over heating, which may cause permanent damage and a shortening of the blade's life time.

Most of the researchers had concentrated on this problem due to the simplicity of geometry, but complexity of the flow structure. Most interesting features are formation of horseshoe vortex and hairpin vortex. Horseshoe vortices are formed due to three dimensional boundary layer separation near the junction of the lower channel wall and the obstacle. When the adverse pressure gradient is significant, the boundary layer separates, wraps around the obstacle and forms a vortex. Its overall shape resembles a horseshoe from which the name of the horseshoe vortex originates.

* Corresponding author. Tel.: +91 44 2257 4063; fax: +91 44 2257 4052.
E-mail address: vengades@iitm.ac.in (S. Vengadesan).

0017-9310/$ - see front matter © 2007 Elsevier Ltd. All rights reserved.
doi:10.1016/j.ijheatmasstransfer.2007.09.029

Nomenclature

h	height of the cube
k	turbulent kinetic energy
u	instantaneous velocity
x, y, z	streamwise, normal and spanwise directions
B	width of the channel
C_p	specific heat
L	length of the channel
LS	line of separation
Re	Reynolds number
Sa	nodal point
St	Stanton number
T_{ref}	reference temperature
U_b	bulk velocity
h_l	local heat transfer coefficient
k_t	thermal conductivity
$\overline{u_i'u_j'}$	Reynolds stresses
y^+	dimensionless distance to wall
C_f	skin friction coefficient
H	height of the channel
LA	line of attachment
Q''_{conv}	convective heat flux
S	symmetric velocity gradient tensor
Sb	saddle point
T_c	cube core temperature
T_{sur}	surface temperature
U_i	mean velocity
Greek symbols	
α	thermal diffusivity
ν	viscosity
ω	turbulent specific dissipation rate
Ω	antisymmetric velocity gradient tensor
ρ	density
ε	turbulent dissipation rate
Δy_{min}	minimum distance from the bottom wall to the first grid point

The flow on the upstream side on the corners of two sides of the block gets branched off in two ways - one flowing upward and the other turning to both sides of the block, then merged together right behind the block to form an arc vortex. This complex structure makes determination of the distributions of the local convective heat transfer a difficult task.

Hunt et al. [1] carried out kinematical studies of the flows around free or surface mounted obstacles by applying topology technique to experimental flow visualizations. Hwang et al. [2] studied numerically the vortical structures around a wall mounted cubic obstacle in a laminar channel flow from low to moderate Reynolds numbers up to 3500. They concluded that flow becomes turbulent in the near wake region at low Reynolds numbers itself. Kim et al. [3] studied the flow and thermal characteristics for the channel with surface mounted heat generating blocks for developing laminar flow. According to them, thermal resistance for the blocks decreases with an increase in Reynolds number and increases in the streamwise direction which is a favorable condition for electronics cooling.

Martinuzzi and Tropea [4] and Hussein and Martinuzzi [5] have done experiment on wall mounted cubic obstacle placed in a fully developed turbulent channel flow at high Reynolds number 40,000. According to them, the blockage ratio is important in determining the total pressure loss. In addition, they also showed that the periodic vortex shedding existed in the wake and the dynamic behavior of the flow in the horseshoe vortex region was bimodal, but non-periodic.

Meinders et al. [6,7] have presented the results of the experimental investigation of the local convective heat transfer from a wall mounted single array of cubical protrusions along a wall of a wind tunnel at $Re = 795$, 2086, 3278 and 5066. According to them, areas of recirculation were accompanied by a minimum heat transfer coefficient, whereas reattachment areas were having higher heat transfer coefficient. Niceno et al. [8] had done the LES simulations on turbulent heat transfer from a multi layered wall mounted cube matrix. Similarly, Verstappen et al. [9] have done the DNS study over the wall mounted matrix of cubes with heat transfer at Reynolds number 5600 based on channel height and bulk velocity. Rodi [10] gave a detailed description on the status of LES. Two test cases namely flow over an infinitely long cylinder and cube in a channel [4] were considered. A large number of LES results with similar boundary conditions were compared by him. He concluded that the flow around the cube was predicted much more accurately than around the square cylinder.

Alexander et al. [11,12] implemented an immersed boundary method to perform a direct numerical simulation (DNS) of flow around a wall mounted cube in a fully developed turbulent channel for a Reynolds number $Re = 5610$, based on the bulk velocity and the channel height. The results confirm the unsteadiness of the flow caused by the unstable interaction of a horseshoe vortex formed in front of the cube and on its both sides with a hairpin vortex behind the cube.

Lakehal and Rodi [13] have done numerical simulations of the flow around a cube placed in a developed channel flow at $Re = 40{,}000$. They have implemented various versions of k–ε model by two layer approach and two versions of one equation models. Iaccarnio et al. [14] studied the same geometry with RANS equations and they showed good agreement with experimental data.

From the foregoing literature study, it is observed that experimental and numerical studies have been reported for surface mounted obstacle for different aspect ratios at

different Reynolds numbers. Most of the researchers have concentrated on aerodynamic study, whereas very few researchers like Meinders et al. [6] and Dinsha et al. [15] have concentrated on heat transfer analysis which has many practical applications. This gives us the motivation to take up the same problem, and evaluate the performance of turbulence model in predicting flow and heat transfer.

2. Objective

Previous studies on the wall mounted cube have been done by using different turbulence models like two layer models, standard k–ε model, DNS and LES. Due to inaccuracy in the prediction by the standard models and high computational cost associated with LES and DNS, we need to arrive at an optimum model which will give accurate results when compared to those by standard models but requires less computational effort when compared to that by LES or DNS. The main objective of the present study is to find out appropriate turbulence model for the geometry shown in Fig. 1 among the available models viz. (1) standard k–ε model (2) low Reynolds number k–ε model [16] (3) non-linear k–ε model [17] (4) Standard k–ω model and (5) An improved k–ω model [18].

3. Formulation of the problem

The physical problem considered in this study is a three-dimensional flow of an incompressible fluid flow around a wall mounted cubic obstacle placed in a channel. Fig. 1 shows the geometry and coordinates chosen for the problem. The case used here is the one that has been studied by Alexander et al. [11]. The height of the channel is three times the cube height ($H/h = 3$). From the literature study, the location of the inflow, outflow and the lateral boundaries is arrived and they are placed at the locations as shown in Fig. 1. The streamwise (L), normal (H), and spanwise (W) lengths of the computational domain are $16h$, $3h$, and $7h$ respectively. In this, x-axis is aligned along the inlet flow direction (streamwise direction), the y-axis is perpendicular to the cube axis (wall-normal direction) and the z-axis is parallel to the cube axis (spanwise direction). The present computations are carried out for Reynolds number of 5610 based on channel height H and bulk velocity U_b and $Re = 1870$ based on cube size and bulk velocity. It is reported in the literature that the flow is turbulent for $Re > 1000$ based on cube size and bulk velocity. Hence the turbulent calculations are appropriate for the present Reynolds number.

3.1. Governing equations

The basic equations used in the present study are incompressible three-dimensional, time dependent; Reynolds averaged Navier–Stokes equations and energy equation. The resulting Reynolds stresses are modeled and the transport equations for standard two equation models are available in standard text books [22,23] and governing equations for low Re k–ε model, non-linear k–ε model and improved k–ω are available in references [16–18] respectively.

3.2. Numerical details

A commercial CFD package FLUENT 6.2.16 is used as a solver to discretize and solve the governing equations. Associated preprocessor GAMBIT 2.2.30 is used for the construction of the computational grid. Fig. 2 shows the computational grid used for the present study. The second order upwind differencing scheme is used for convective terms and terms in equations for turbulent quantities and energy equation. Second order central differencing scheme is adopted for diffusion terms. SIMPLE (semi implicit method for pressure linked equation) algorithm is used for coupling the pressure and velocity terms. Second order

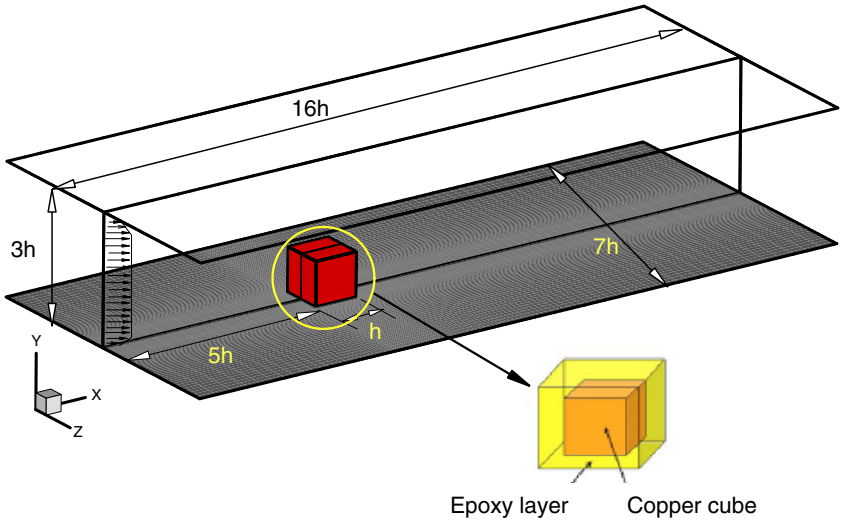

Fig. 1. Schematic sketch and computational domain of the present study.

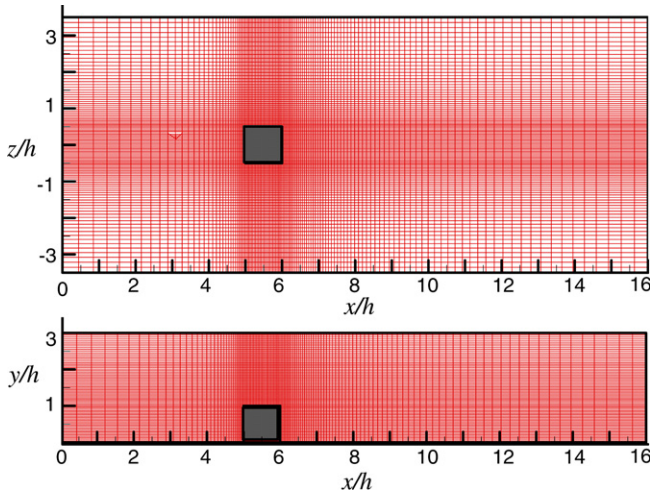

Fig. 2. Computational grid used for the present study.

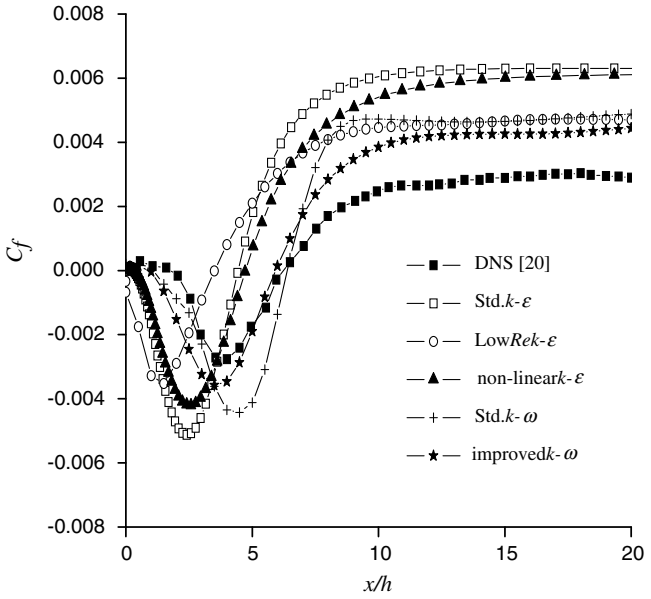

Fig. 3. Comparison of skin friction coefficient along the bottom wall of the BFS.

Table 1
Summary of reattachment length for BFS

Models	Reattachment length (x_r/h)	Deviation (%)
DNS [20]	6.28	–
Standard k–ε	5.6	11
Low*Re* k–ε	3.58	40
Non-linear k–ε	5.8	7
Standard k–ω	6.0	4.8
Improved k–ω	6.2	1.3

implicit scheme is used for time advancement. While standard models and low *Re* models are available in FLUENT, non-linear k–ε model and improved k–ω model are incorporated in FLUENT through user defined functions (UDFs). The non-linear term is added as a source term for k, ε equations and cross diffusion term is added as a source term in ω equation. The turbulent viscosity is also made to vary as per the respective relation through UDFs. The implementation of the non-linear k–ε model was validated for turbulent flow around a square cylinder [19]. The non-linear k–ε model along with improved k–ω model are validated against benchmark case (DNS by Le et al. [20]) of flow through the backward facing step (BFS) at $Re = 5100$, based on the step height, h. Table 1 gives summary of the reattachment length by two equation eddy viscosity models and Fig. 3 shows the comparison of normalized skin friction coefficient on the bottom wall. Figure shows high levels of skin friction in the reversed flow region which is an indication of the energetic mixing resulting in steep velocity gradient near the wall. Predictions by the improved k–ω model match well with DNS with 1.3% of error. After the reattachment point, all other two equation turbulence models overpredict.

3.3. Boundary conditions

A fully developed turbulent velocity profile with a bulk velocity U_b and a uniform temperature $T_{ref} = 20$ °C is prescribed at the channel inlet. The structure of the cube is decomposed into two materials as shown in Fig. 1; the core of the cube is constructed from copper which is kept at constant temperature $T_c = 75$ °C. The second material is an Epoxy resin which encapsulated the copper and has a uniform thickness of $0.1h$. Other physical properties taken from the experimental report [6] are summarized in Table 2. The temperature in the Epoxy layer is governed by an unsteady diffusion equation. Coupled boundary condition is given on the Epoxy layer. No-slip boundary condition is applied on all faces of the cubic obstacle and convective boundary condition is specified at the exit boundary. Periodic boundary condition is employed in the spanwise direction.

Table 2
Physical properties of air and Epoxy resin

Property symbol	Air	Epoxy
C_p (m^2/s^2 K)	1007.0	1668.5
α (m^2/s)	2.197×10^{-5}	1.230×10^{-7}
k_t (kg m/s^2 K)	0.0257	0.236
ρ (kg/m^3)	1.16	1150.0

3.4. Solution convergence

The convergence of the computational solution is determined based on scaled residuals for the continuity, momentum and energy equations. The scaled residuals for solution convergence are set to 10^{-5} for all governing equations except the energy equation. The residual for energy equation is set to 10^{-8}. The solution is considered to be converged when all of the scaled residuals are less than or equal to this prescribed value.

Computations are carried out until the steady state is reached. The grid is finer near the surface of the cube in all directions and near the bottom wall. The first cell adjacent to the walls was to satisfy the criteria required for the individual near wall treatment. Hence, when using wall functions for high *Re* model, the width of the near wall cell was 0.008H and when using the damping functions for low *Re* model the width of the near-wall cell was 0.001H, which corresponds to $10 < y^+ < 25$ and $1 < y^+ < 7$, respectively. In low Reynolds turbulence model cases, the numbers of grid points placed in the viscous sublayer are typically 10–15. Grid independence study was carried out to reduce the uncertainties associated with mesh. Calculations showed that grid independent results could be obtained for standard turbulence models with $114 \times 60 \times 78$ grid size and for low Reynolds number turbulence models with $132 \times 70 \times 100$ grid size and results by these grids are reported here.

4. Results and discussion

A detailed numerical study of three-dimensional unsteady incompressible flow over a wall mounted cube is carried out with fully developed turbulent velocity profile as inlet condition. Unsteady calculations are advanced with non-dimensional time step of 0.001 and final solutions are obtained for minimum of 68,955 time steps. Averaging is done for over 50 vortex shedding cycles which is observed at $z/h = 0$, $x/h = 6$, $y/h = 0.5$ from the obstacle. Fig. 4 shows the comparison of time

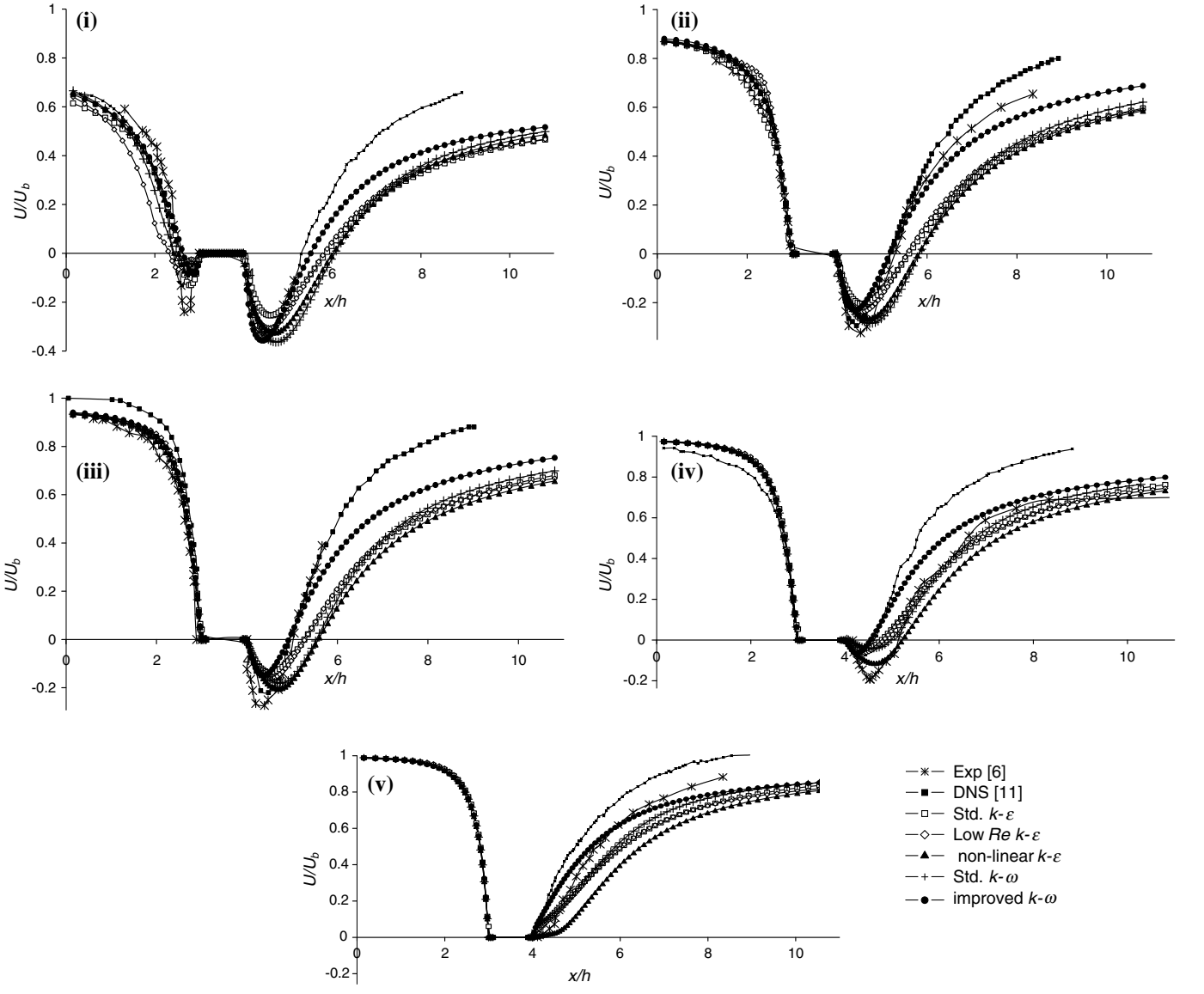

Fig. 4. Comparison of mean streamwise velocity profiles in the symmetry line; (i) $y/h = 0.1$, (ii) $y/h = 0.3$, (iii) $y/h = 0.5$, (iv)$y/h = 0.7$ and (v) $y/h = 0.9$ Legends are same in all the plots.

averaged streamwise velocity profiles at various y/h positions on the symmetry plane with DNS [11] and experiment by Meinders et al. [6]. Experiment is carried out at relatively higher Reynolds number 2750 based on cube size and bulk velocity. Streamwise velocity is normalized by the bulk velocity U_b. In the front recirculation and reattachment regions, results by improved k–ω and non-linear k–ε models show better agreement with DNS [11] and the experimental results by Meinders et al. [6]. In the redeveloping region, though they slightly overpredict, the deviation from DNS is less when compared to prediction by other eddy viscosity models. Hence here afterwards, we are presenting the results by improved k–ω and non-linear k–ε models, and comparison with the DNS [11] and experiment [6].

4.1. Streamlines pattern and skin friction coefficient

Streamlines are used to visualize separations, recirculation and reattachments in the mean flow in front, on the top of, along the lateral sides and behind the cube. Fig. 5 shows the comparison with DNS [11], the time averaged

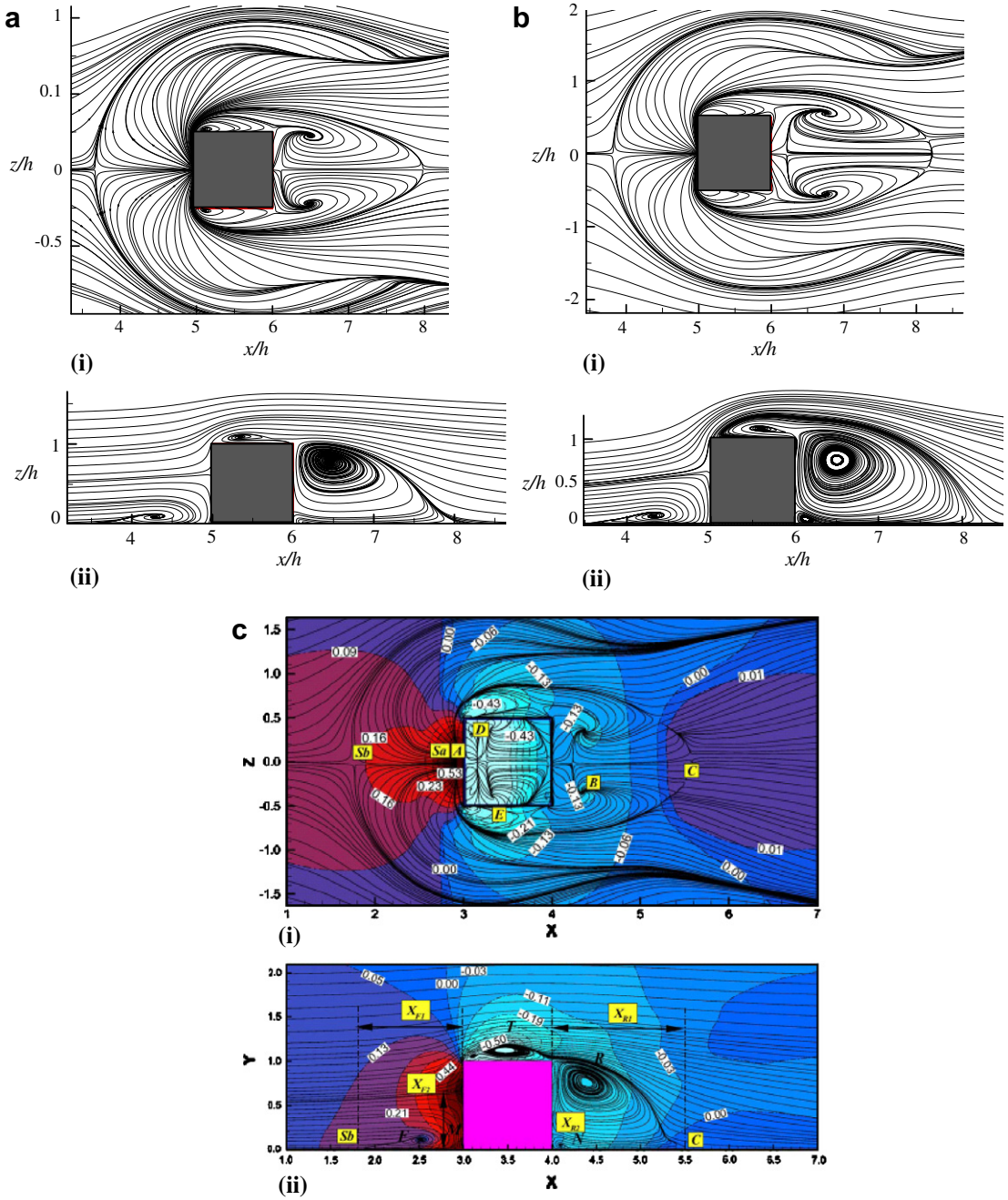

Fig. 5. Comparison of time averaged streamlines on (i) first grid point from the lower wall, (ii) the central plane ($z/h = 0$); (a) non-linear k–ε, (b) improved k–ω and (c) DNS [11].

Table 3
Summary of front separation (X_{F1} and X_{F2}), reattachment (X_{R1} and X_{R2}) and top recirculation lengths (X_t) for a wall mounted cube by different turbulence models

Turbulence model	X_{F1}	X_t	X_{R1}	X_{F2}	X_{R2}
DNS [11]	1.2	0.5	1.5	0.6	0.15
Standard k–ε	0.8	0.4	2.2	0.58	0.18
Low Re k–ε	1.58	0.6	2.3	0.6	0.15
Non-linear k–ε	1.5	0.55	2.0	0.6	0.13
Standard k–ω	1.4	0.3	2.2	0.55	0.2
Improved k–ω	1.29	0.5	2.2	0.6	0.15

streamlines and the pressure distribution (back ground color[1]) on the first grid point from the bottom wall and on the symmetry plane. There is a horseshoe vortex in front of the cube, recirculation regions on the top (marked as T) and behind the cube (marked as R). These vortices look similar to those by DNS [11]. All marked points in this figure correspond to those used in DNS study as well as in the oil film visualization by Meinders et al. [6]. In Fig. 4, one can clearly see that the flow gets separated at a point far upstream of the obstacle called a saddle point (marked as *Sb*). We can also observe an attachment point just in front of the cube and this is called as a nodal point (marked as *Sa*). For a detailed description of the saddle and nodal points, see Ref. [4].

The streamlines which pass through *Sb* go around the obstacle form a "line of separation LS" on the lower wall. Since the formation of horseshoe vortex is preceded by flow separation, it is confined inside the corresponding LS. The streamlines approaching *Sa* form "line of attachment LA". The extent of streamwise vortical structure in the downstream of the obstacle is bounded by LA and LS. There are also closely spaced but not clearly visible nodal and saddle points on the upstream side of the obstacle. These are caused by the presence of the secondary vortices. The two nodal points symmetrically located downstream of the obstacle are referred as foci of separation (marked as B). The flow from the upstream side approaches these points in a spiral fashion and simultaneously moves upwards to form arch vortex. In the rear of the cube, the shear layer that is separated at the top leading edge reattaches at approximately $2.2h$ downstream of the trailing face (marked as C), whereas reported reattachment length by DNS is $1.5h$. One of the reasons for deviation in our prediction could be due to stretching of mesh in the streamwise direction. The lengths of front recirculation length X_{F1}, top recirculation X_t, reattachment length X_{R1} and secondary recirculation lengths X_{F2}, and X_{R2} are given in the Table 3.

4.2. Streamwise vorticity pattern

To estimate the horseshoe vortex size, we show in Fig. 6 the front view of the time averaged streamwise vorticity Ω_x contour plots in the vicinity of the cube at different streamwise x/h locations. Only the contours associated with the horseshoe vortex are shown in Fig. 6. The converging–diverging nature of the horseshoe vortex can be observed and its cross-stream size increases with the increase of x/h, but does not exceed $0.35h$ by both the models. The horseshoe vortex is detached from the cube; its distance from the side faces Z_h and its height Y_h increases. This increase rate is more intensive from $x/h = 5.1$ to $x/h = 5.5$ than from $x/h = 5.5$ to $x/h = 5.9$. At $x/h = 5.9$, the vortex extends until about $Z_h = 0.45h$ and $Y_h = 0.35h$. Improved k–ω model gives better agreement with DNS. Fig. 7 shows time averaged volume lines from which we can see the main vortical structures clearly. The volume lines predicted by both the models are very similar to DNS [11] as well as the artist's impression sketch of the flow structure presented in Meinders et al. [6].

4.3. Reynolds stress on the symmetry plane

Fig. 8 shows the normalized Reynolds stresses $\overline{u'^2}$ and $\overline{u'v'}$ in the symmetry plane. The Reynolds stresses are calculated by using Bussinesq approximation.

$$-\overline{u_i'u_j'} = v_t\left(\frac{\partial U_i}{\partial x_j} + \frac{\partial U_j}{\partial x_i}\right) - \frac{2}{3}k\delta_{ij}.$$

Non-linear k–ε and improved k–ω models are showing better agreement with DNS [11]. The contours depict the Reynolds stress enhancement in the recirculation region over the cube's top face. The local maxima of $\overline{u'v'}$ is clearly observed in front of the cube.

The time averaged turbulent kinetic energy contours in the x–z plane at $y/h = 0.1$, 0.25 and 0.5 are shown in Fig. 9. From the figure, we can say that the enhancement of turbulent production occurs in horseshoe vortex. It should be also noted that the distribution of turbulent kinetic energy in the recirculation region on the rear side is quasi two-dimensional (i.e. y independent).

4.4. Second invariant of velocity gradient

Hunt et al. [21] had defined an "eddy structure" as a positive second invariant of velocity gradient. This is given as

$$Q = -\frac{1}{2}\frac{\partial U_i}{\partial x_j}\frac{\partial U_j}{\partial x_i} = -\frac{1}{2}\left(S_{ij}S_{ij} - \Omega_{ij}\Omega_{ij}\right).$$

This method was used to view the complex vortical structures in the mean flow as well as in the instantaneous flow. The isosurfaces of time averaged $Q = 0.2$ is shown in Fig. 10. Both horseshoe vortex in front of the cube and arch vortex after the cube can be seen. An improved k–ω model is giving clear vortical structure when compared to non-linear k–ε model.

4.5. Time averaged temperature plots

The profiles of surface temperatures along two representative paths ABCDA and A′B′C′D′ are shown in Fig. 11

[1] For interpretation of color in Fig. 5, the reader is referred to the web version of this article.

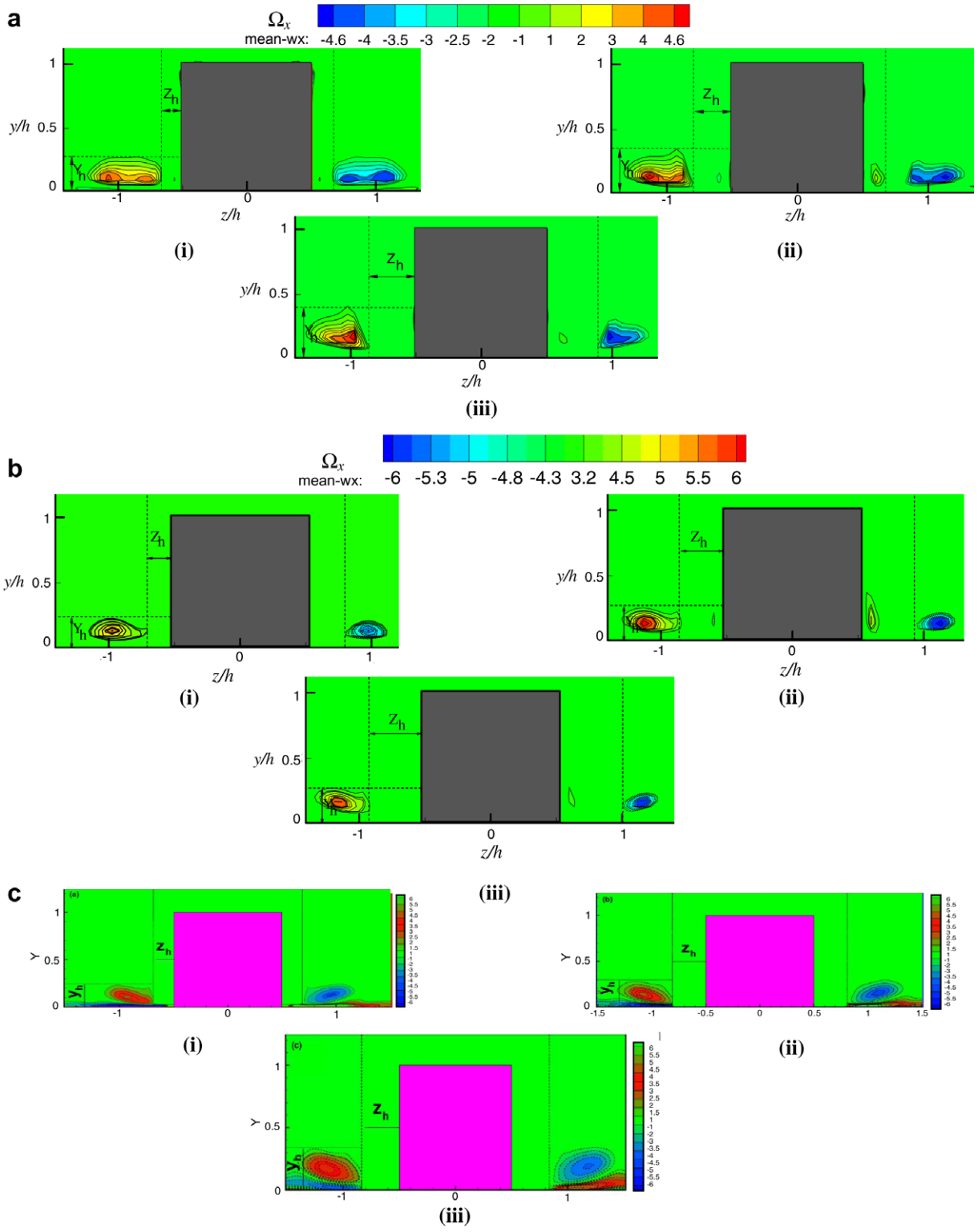

Fig. 6. Comparison of time averaged stream wise vorticity contours on (i) $x/h = 5.1$, (ii) $x/h = 5.5$ and (iii) $x/h = 5.9$; (a) non-linear k–ε, (b) improved k–ω and (c) DNS [11].

comparing with the experimental results by Meinders et al. [6]. As it can be observed in the experimental results, the surface temperature is decreasing with increase of Reynolds number. Since we are doing with relatively lower Re (=1870) than that referred in the experiment, the temperature distribution in the present case should be higher than that of experimental results. Results by standard k–ω and improved k–ω models are following the trend of experimental results. Figs. 12(i) and 12(ii) show the contours of the surface temperature, and local heat transfer coefficient,

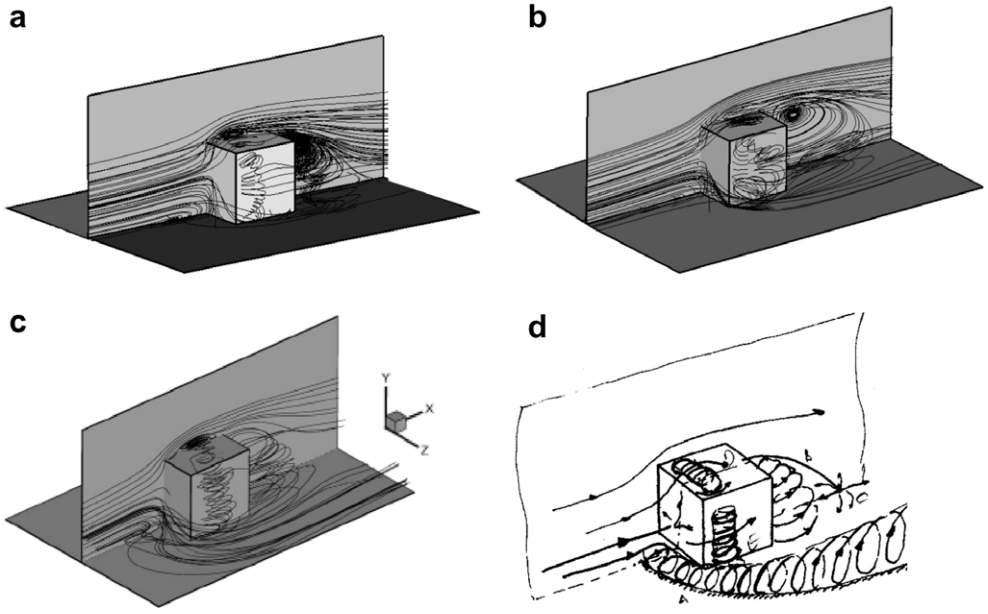

Fig. 7. Time averaged volume lines; (a) non-linear k–ε, (b) improved k–ω, (c) DNS [11] and (d) Ref. [6].

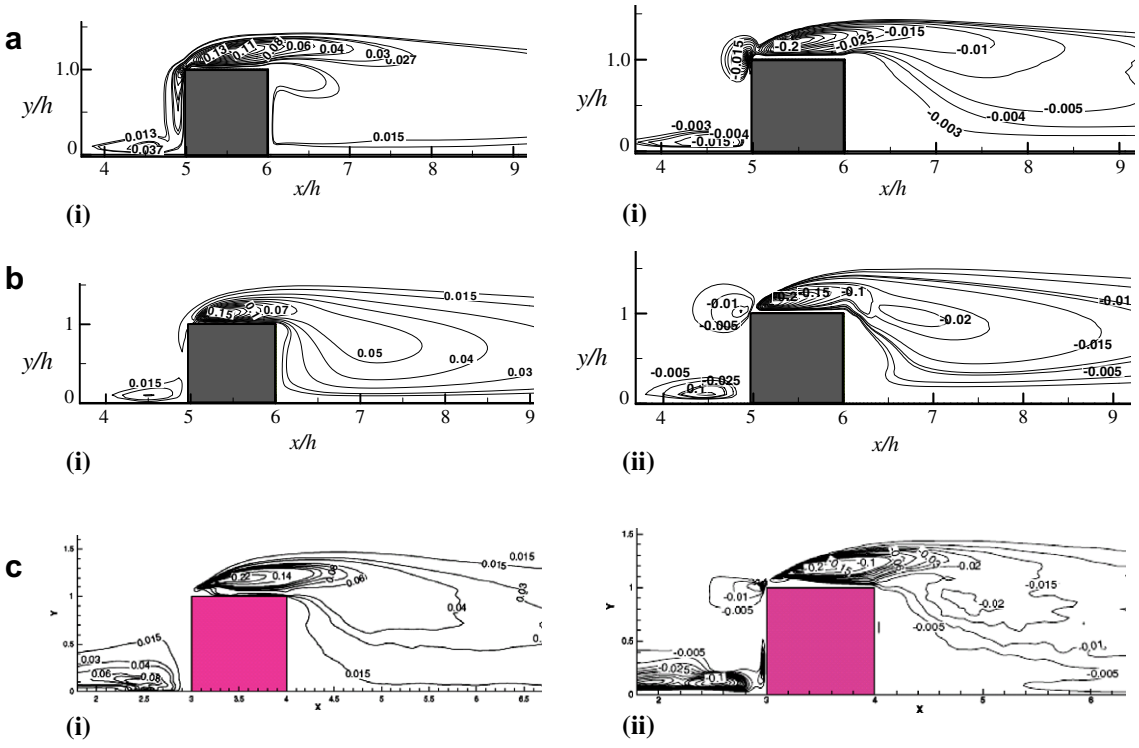

Fig. 8. Comparison of (i) streamwise normal stress $\overline{u'^2}/u_b^2$ and (ii) shear stress $\overline{u'v'}/u_b^2$ contours on the symmetry plane; (a) non-linear k–ε, (b) improved k–ω and (c) DNS [11].

h_1 respectively on the cube faces. From the Fig. 12(i), it is observed that the minimum temperature occurs on the faces BC and C′D′ along the paths ABCDA and A′B′C′D′ respectively.

The h_1 is calculated according to the formula given below

$$h_l = \frac{Q''_{\text{conv}}}{T_{\text{sur}} - T_{\text{ref}}}.$$

Surface temperature will be more on the recirculation zones since the rotational behaviour of the vortex causes the residence time of the fluid in the vortex to be high, allowing

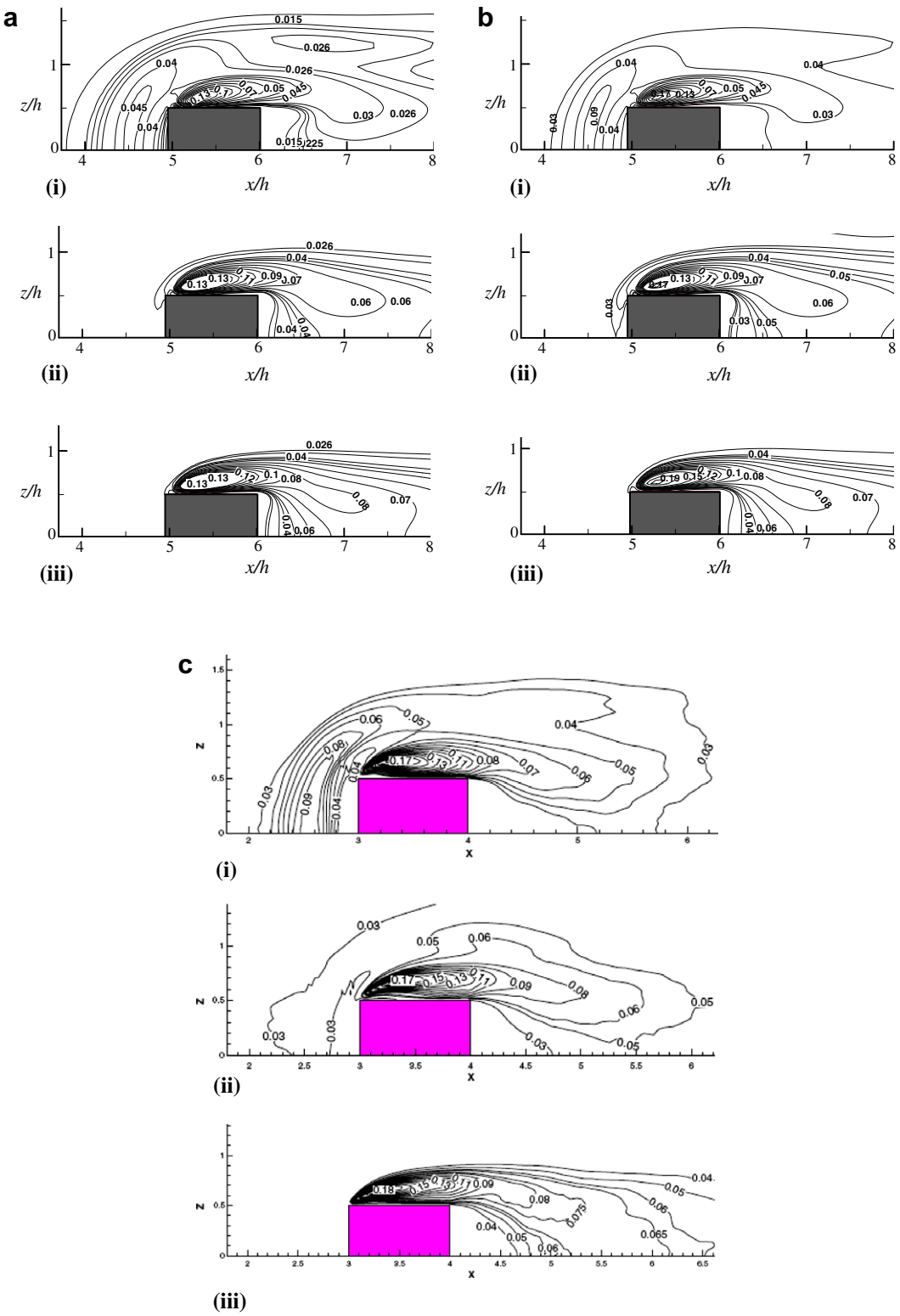

Fig. 9. Comparison of mean turbulent kinetic energy in the xz plane; (i) $y/h = 0.1$, (ii) $y/h = 0.25$, (iii) $y/h = 0.5$; (a) non-linear k–ε, (b) improved k–ω and (c) DNS [11].

the local fluid temperature to increase and in turn reducing the local heat transfer coefficient.

The convective heat transfer from the leeward face of the cube is almost uniform. The flow on this face is dominated by the arch vortex. Due to the mechanism of vortex shedding, the recirculation of fluid in the wake resulted intense mixing which led to higher and uniform distribution of local fluid temperature. A local minimum of heat transfer coefficient

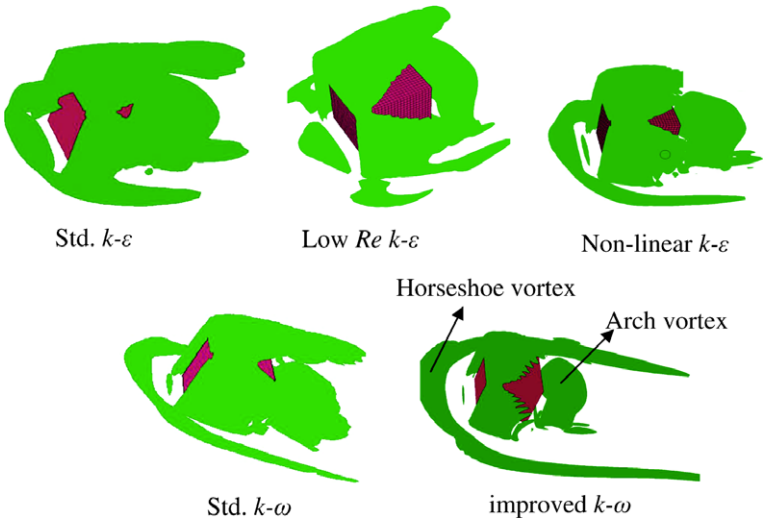

Fig. 10. Time averaged second invariant of the velocity gradient $Q = 0.2$.

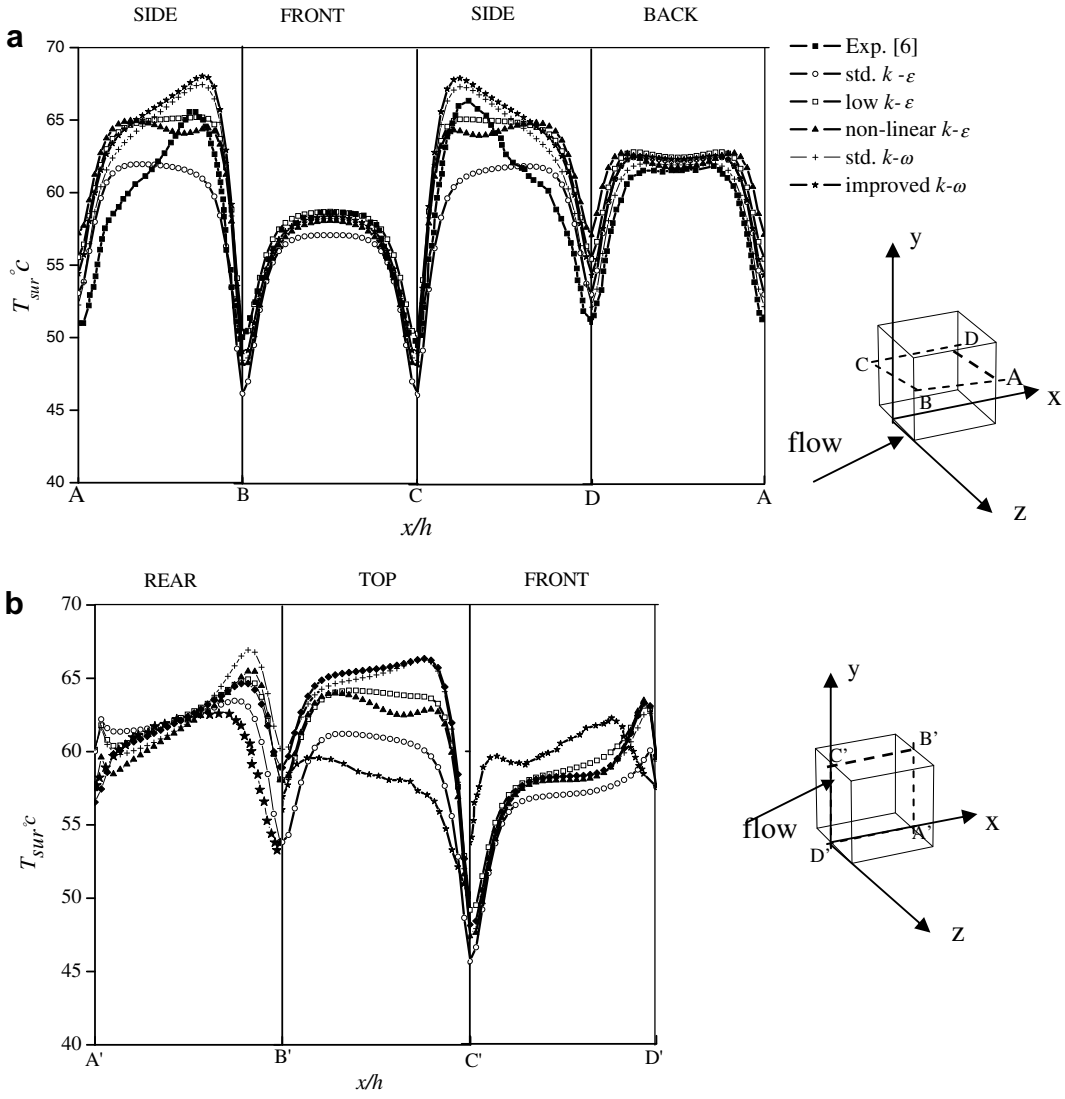

Fig. 11. Surface temperature distribution along the paths (a) ABCDA and (b) A′B′C′D′. Legends are same in both the plots.

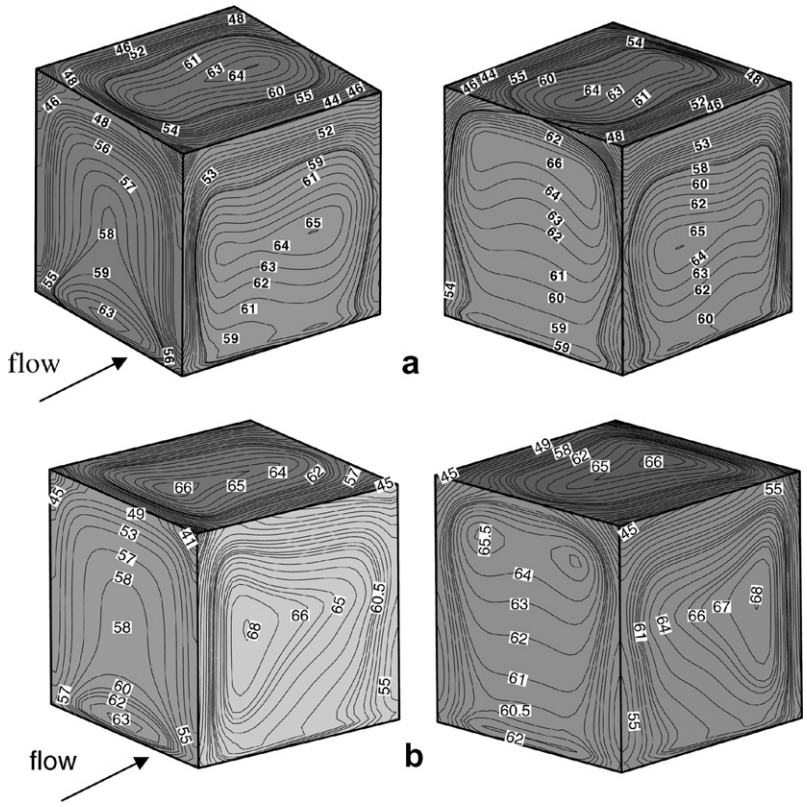

Fig. 12(i). Contours of surface temperature on cube faces; (a) non-linear k–ε and (b) improved k–ω.

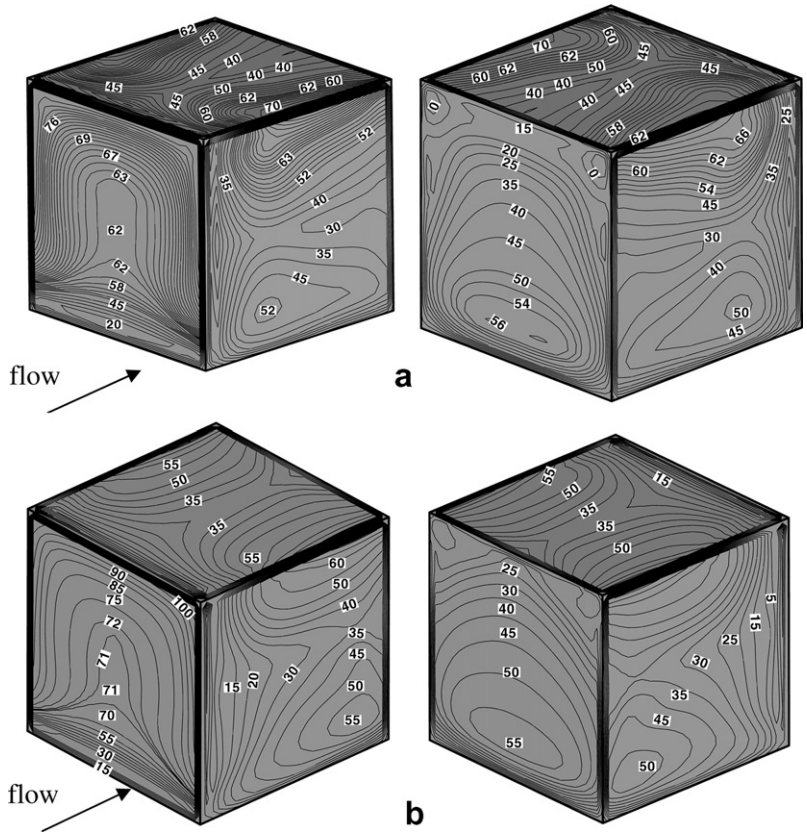

Fig. 12(ii). Contours of local heat transfer coefficient, h_l on the cube faces; (a) non-linear k–ε and (b) improved k–ω.

on the side faces is found on the upstream part of the side face and a local maximum exists downstream close to the trailing side edge. St is increased slightly on side faces of the cube in streamwise direction. Similar to the side faces, the vortex over the top face dictates the local heat transfer coefficient. A local heat transfer minimum observed in an area of high wall shear stress (on the wall directly below the bound vortex) and a local maximum in the area of low-wall shear stress (reattachment region).

5. Conclusions

In this study, numerical simulations are carried out to elucidate the characteristics of the vortical structures and heat transfer coefficient associated with a cubic obstacle mounted on one wall of the channel. Calculations are carried out by using five turbulence models. Results showed that the improved k–ω model is showing better agreement with DNS as well as the experimental study and non-linear k–ε models is giving better predictions than that of Std. k–ε and low Re k–ε models. The converging–diverging nature of the horseshoe vortex can be observed and its cross-stream size increases with the increase of x/h, but does not exceed $0.35h$ by both the models and this value is consistent with DNS [11]. The maximum heat transfer coefficient occurred in the proximity of reattachment points; whereas minimum heat transfer coefficient is found in the recirculation zone.

References

[1] J.C.R. Hunt, J.A. Peterks, C.J. Abell, H. Woo, Kinematical studies of the flows around free or surface mounted obstacles; Applying topology to flow visualization, J. Fluid Mech. 86 (1978) 179–191.
[2] J.Y. Hwang, Y. Hyung Soo, Numerical study of vortical structures around a wall-mounted cubic obstacle in channel flow, Phys. Fluids 16 (7) (2004) 2383–2394.
[3] S.H. Kim, N.K. Anand, Laminar developing flow and heat transfer between a series of parallel plates with surface mounted discrete heat sources, Int. J. Heat Mass Transfer 37 (15) (1994) 2231–2244.
[4] R. Martinuzzi, C. Tropea, The flow around surface-mounted prismatic obstacles placed in a fully developed channel flow, Trans. ASME J. Fluid Eng. 115 (1) (1993) 85–91.
[5] H.J. Hussein, R.J. Martinuzzi, Energy balance for turbulent flow around a surface mounted cube placed in a channel, Phys. Fluids 8 (3) (1996) 764–780.
[6] E.R. Meinders, K. Hanjalic, R. Martinuzzi, Experimental study of the local convective heat transfer from a wall mounted cube in turbulent channel flow, Trans ASME J. Heat Transfer 121 (1991) 564–573.
[7] E.R. Meinders, K. Hanjalic, Experimental study of the convective heat transfer from in line and staggered configurations of two wall mounted cubes, Int. J. Heat Mass Transfer 45 (2002) 465–482.
[8] B. Niceno, A.D.T. Dronkers, K. Hanjalic, Turbulent heat transfer from a multi-layered wall mounted cube matrix: a large eddy simulation, Int. J. Heat Fluid Flow 23 (2002) 173–185.
[9] R.W.C.P. Verstappen, R.M. Vander Velde, A.E.P. Veldman, DNS of turbulent flow and heat transfer in a channel with surface mounted cubes, European Congress on Computational Methods in Applied Sciences and Engineering, Barcelona, September 2000.
[10] W. Rodi, Comparison of LES and RANS calculations of the flow around bluff bodies, J. Wind Eng. Ind. Aerodyn. 69 (71) (1997) 55–75.
[11] Y. Alexander, H. Liu, N. Nikitin, Turbulent flow around a wall mounted cube: A direct numerical simulation, Int. J. Heat Fluid Flow 27 (2006) 994–1009.
[12] Y. Alexander, H. Liu, N. Nikitin, DNS of turbulent flow around a wall mounted cube: Spatio-temporal evolution of large-scale vortices, J. Fluid Mech. 566 (2006) 1–9.
[13] D. Lakehal, W. Rodi, Calculation of the flow past a surface mounted cube with 2 layer turbulence models, J. Wind Eng. Aerodyn. 67–68 (1997) 66–78.
[14] G. Iaccarnio, A. Ooi, M. Behina, Reynolds averaged simulation of unsteady separated flow, Int. J. Heat Fluid Flow 24 (2003) 147–156.
[15] K.K. Dhinsa, C.J. Bailey, K.A. Pericleous, Turbulence modeling and its impact on CFD predictions for cooling of electronic components, Inter Society Conference on Thermal Phenomena, 2004.
[16] R. Abid, Evaluation of two equation turbulence models for predicting transitional flows, Int. J. Eng. Sci. 32 (6) (1993) 831–840.
[17] I. Kimura, T. Hosoda, A non-linear k–ε model with realizability for prediction of flows around bluff bodies, Int. J. Numer. Methods Fluids 42 (2003) 817–837.
[18] J. Bredberg, S.H. Peng, L. Davidson, An improved k–ω turbulence model applied to recirculating flows, Int. J. Heat Fluid Flow 23 (2002) 731–743.
[19] V. Ramesh, S. Vengadesan, J.L. Narasimhan, 3D Unsteady RANS simulations of turbulent flow over bluff body by non-linear model, Int. J. Numer. Methods Heat Fluid Flow 16 (6) (2006) 660–673.
[20] H. Le, P. Moin, J. Kim, Direct numerical simulation of turbulent flow over a backward facing step, J. Fluid Mech. 330 (1997) 349–375.
[21] J.C.R. Hunt, A.A. Wray, P. Moin, Eddies, stream, and convergence zones in turbulent flows, Center for Turbulence Research Report CTR S88 (1988) 193.
[22] D.C. Wilcox, Turbulence Modeling for CFD, third ed., DCW Industries, 2006.
[23] S.B. Pope, Turbulent Flows, fourth ed., Cambridge University Press, 2005.